PRINCIPAL OSCILLATION PATTERN ANALYSIS OF THE INTRASEASONAL VARIABILITY IN THE EQUATORIAL PACIFIC OCEAN

Hans von Storch
Max-Planck-Institut für Meteorologie, Hamburg, Germany

ABSTRACT

In the present paper the concept of the *principal oscillation pattern* (POP) analysis is reviewed. This technique is used to simultaneously infer the characteristic patterns and time scales of a vector time series. The POPs may be seen as the normal modes of a linearized system whose system matrix is estimated from data. As a demonstration, the POP technique is used for the analysis of the intraseasonal variability in the equatorial Pacific Ocean; first results are presented. Daily observations of temperature and currents in the upper 500 m of the equatorial Pacific, recorded by moored buoys, are analyzed with respect to intraseasonal (40-180 day band) variations. Two oscillatory highly coherent modes are found with periods between 65 and 120 days. Both modes propagate eastward along the equator. The modes are clearly reflected in both the zonal currents and the temperatures, which trail behind the zonal currents by 45°. In the slower of the two modes, the temperature signal propagates more slowly than the zonal current signal, and no signal occurs in the meridional current. The mode's activity is enhanced during warm events of the Southern Oscillation. In the faster mode a signal also appears in the meridional current. Its amplitude exhibits an annual cycle, with variance on the annual and on the semiannual period. The slower mode might be an equatorial Kelvin wave but the faster mode, which has a significant meridional current component, is inconsistent with the concept of an equatorial Kelvin wave.

1. INTRODUCTION

Principal oscillation pattern analysis. In the present paper the *principal oscillation pattern* (POP) technique is reviewed (Section 2) and its usefulness is demonstrated by an analysis of the intraseasonal variability in the equatorial Pacific (Section 3). The POP analysis is a multivariate technique to empirically infer the characteristics of the space-time variations of a complex system in a high-dimensional space (Hasselmann, 1988; von Storch et al., 1988). The basic ansatz is to identify a low-order system with a few free parameters fitted to the data. Then, the space-time characteristics of the low-order system are regarded as being the same as those of the full system.

Applications of POP analysis. The POP analysis is now a routinely used tool[1] to diagnose the space-time variability of the climate system. Processes analysed with POPs are

- The low-frequency variability of the thermohaline circulation in the global ocean (Mikolajewicz and Maier-Reimer, 1991; Weisse et al., in press),
- The low-frequency variability in the coupled atmosphere-ocean system (Xu, 1993),
- The El Niño / Southern Oscillation ENSO (Xu and von Storch, 1990; Xu, 1990; Blumenthal, 1991; Latif and Villwock, 1989; Latif and Flügel,1990; Bürger, 1993; Xu, 1992; Latif et al., 1993),
- The Madden and Julian Oscillation (MJO), also named the tropical 30- to 60-day oscillation (von Storch et al., 1988; von Storch and Xu,1990; von Storch and Baumhefner, 1991; and von Storch and Smallegange,1991),
- The stratospheric Quasi-Biennial Oscillation (Xu, 1992),
- Tropospheric baroclinic waves (Schnur et al., 1993).

Generalizations of the POP analysis. There is a series of generalizations of the basic POP approach which we will not detail in the present paper. The predictive potential of the POP method has been tested with the Southern Oscillation (Xu and von Storch, 1990) and with the Madden and Julian Oscillation (von Storch and Xu, 1991). In the *cyclo-stationary* POP analysis, the estimated system matrix is allowed to vary deterministically with an externally forced cycle (Blumenthal, 1991). In the *complex* POP analysis not only the state of the system but also its "momentum" is modeled (Bürger, 1993).

Organization. In Section 2, the POPs are introduced in two conceptually different ways. One way is to define POPs as normal modes of a linear system in which parameters are inferred from a vector time series. The other way is to regard POPs as a simplified version of principal interaction patterns (PIPs). The PIP ansatz (Hasselmann, 1988) is a fairly general approach which allows for a large variety of complex scenarios. In Section 3 a POP analysis of daily hydrographic reports (temperature, zonal and meridional currents, as well as surface wind) from moored buoys in the tropical Pacific Ocean is presented. Two eastward propagating modes, both similar to the mode described by Johnson and McPhaden (1993), are identified and their spatial signatures are described. The paper is concluded in Section 4 with some remarks on the general merits and limitations of the POP technique.

[1]A FORTRAN code with a manual (Gallagher et al., 1991) of the regular POP analysis is free of charge available at the Deutsches Klimarechenzentrum, Bundesstrassse 55, 2000 Hamburg 13, Germany.

2. PRINCIPAL OSCILLATION PATTERNS

The following notations are used: Vectors are given as **bold** letters and matrices as calligraphic letters like $\mathcal{A}$ or $\mathcal{X}$. If $\mathcal{A}$ is a matrix then $\mathcal{A}^T$ is the transposed matrix. If x is any complex quantity then x^* is its conjugate complex. It should be noted that the POP formalism—conventional, cyclostationary, and complex POP analysis—may be applied to linear systems whose system matrices are estimated from data or whose system matrices are derived from theoretical dynamical considerations (Schnur et al., 1993).

2.1 POPs and Normal Modes

Normal modes. The normal modes of a linear discretized real system

$$\mathbf{x}(t+1) = \mathcal{A} \cdot \mathbf{x}(t) \tag{1}$$

are the eigenvectors $\mathbf{p}$ of the matrix $\mathcal{A}$. In general, $\mathcal{A}$ is not symmetric and some or all of its eigenvalues λ and eigenvectors $\mathbf{p}$ are complex. However, since $\mathcal{A}$ is a real matrix, the conjugate complex quantities λ^* and $\mathbf{p}^*$ satisfy also the eigen-equation $\mathcal{A} \cdot \mathbf{p}^* = \lambda^* \mathbf{p}^*$. In most cases, all eigenvalues are different and the eigenvectors form a linear basis. So each state $\mathbf{x}$ may be uniquely expressed in terms of the eigenvectors

$$\mathbf{x} = \sum_j z_j \cdot \mathbf{p}_j . \tag{2}$$

The coefficients of the pairs of conjugate complex eigenvectors are conjugate complex, too. Inserting (2) into (1) we find that the coupled system (1) becomes uncoupled, yielding n single equations, where n is the dimension of the process $\mathbf{x}$,

$$z(t+1) \cdot \mathbf{p} = \lambda \cdot z(t) \cdot \mathbf{p} \tag{3}$$

so that if $z(0) = 1$

$$z(t) \cdot \mathbf{p} = \lambda^t \cdot \mathbf{p} . \tag{4}$$

The contribution $\mathbf{P}(t)$ of the complex conjugate pair $\mathbf{p}$, $\mathbf{p}^*$ to the process $\mathbf{x}(t)$ is given by

$$\mathbf{P}(t) = z(t) \cdot \mathbf{p} + [z(t) \cdot \mathbf{p}]^* . \tag{5}$$

Writing $\mathbf{p} = \mathbf{p}^1 + i \cdot \mathbf{p}^2$ and $2z(t) = z^1(t) - i \cdot z^2(t)$, this reads

$$\begin{aligned} \mathbf{P}(t) &= z^1(t) \cdot \mathbf{p}^1 + z^2(t) \cdot \mathbf{p}^2 \\ &= \rho^t \cdot (\cos(\eta t) \cdot \mathbf{p}^1 - \sin(\eta t) \cdot \mathbf{p}^2) \end{aligned} \tag{6}$$

with $\lambda = \rho \cdot \exp(-i\eta)$ and if $z(0) = 1$. The geometric and physical meaning of (6) is that between the spatial patterns $\mathbf{p}^1$ and $\mathbf{p}^2$ the trajectory $\mathbf{P}(t)$ performs a spiral (Figure 1) with period $T = 2\pi/\omega$ and e-folding time $\tau = -1/\ln(\rho)$, in the consecutive order

$$\cdots \rightarrow \mathbf{p}^1 \rightarrow -\mathbf{p}^2 \rightarrow -\mathbf{p}^1 \rightarrow \mathbf{p}^2 \rightarrow \mathbf{p}^1 \rightarrow \cdots \tag{7}$$

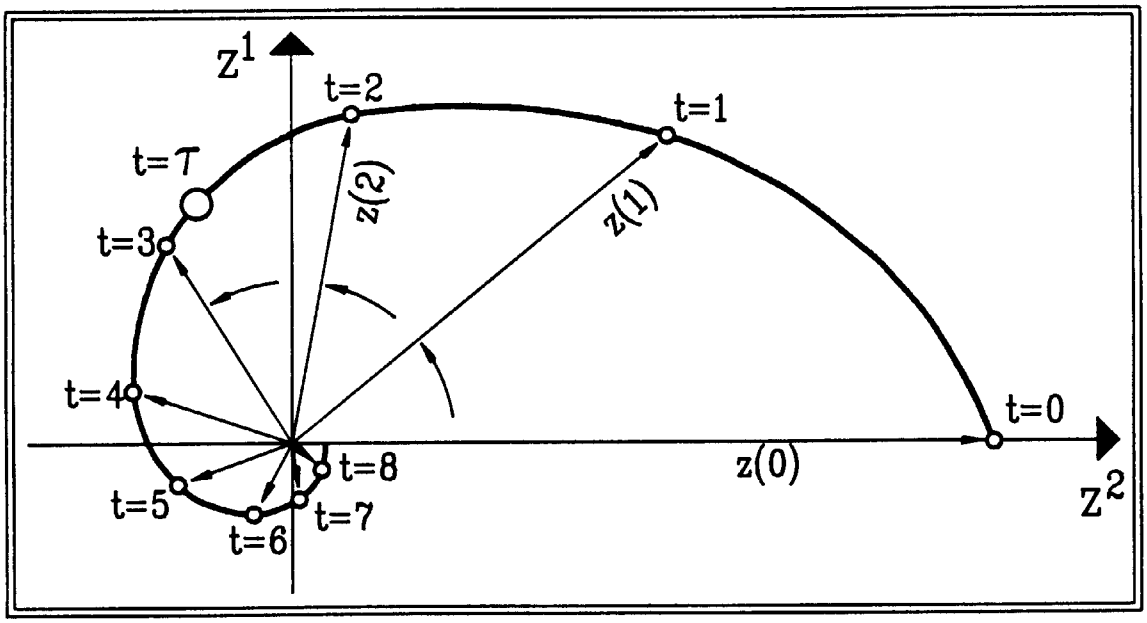

Figure 1. Typical evolution of a POP signal, given by Eq. (6), if $z^1(0) = 0$ and $z^2(0) = 1$. In this demonstration the period is $T \approx 9$ and the e-folding time is $\tau \approx 2.8$.

The e-folding time. The e-folding time has to be considered with some caution. It represents formally the average time for an amplitude of strength one to reduce to $1/e$. But in the POP context this time is a statistic of the entire time interval, i.e., it is derived not only from the episodes when the signal is active but also from those times when the signal is weak or even absent. As such, the mode will be dampened less quickly as indicated by the e-folding time when the mode is active. The other limitation refers to the presence or absence of high-frequency variations. If these are filtered out, as in Section 3, the e-folding time is lengthened.

Representation of normal modes. The modes may be represented either by the two patterns $\mathbf{p}^1$ and $\mathbf{p}^2$, or by plots of the local wave amplitude $A^2(\mathbf{r}) = [\mathbf{p}^1(\mathbf{r})]^2 + [\mathbf{p}^2(\mathbf{r})]^2$ and relative phase $\psi(\mathbf{r}) = \tan^{-1}[\mathbf{p}^2(\mathbf{r})/\mathbf{p}^1(\mathbf{r})]$ (Figure 2). The transformation (7) between the patterns $\mathbf{p}^1$ and $\mathbf{p}^2$ can assume various geometric wave forms. If $\mathbf{p}^2(\mathbf{r}) = \mathbf{p}^1(\mathbf{r} - \mathbf{r}_0)$ with a location vector $\mathbf{r}$ and a fixed vector $\mathbf{r}_0$, the signal appears as a parallel crested wave of

wavelength $4\mathbf{r}_0$, propagating in the $\mathbf{r}_0$-direction (Figure 2a). In Figure 2b an amphidromal (rotational) wave is shown.

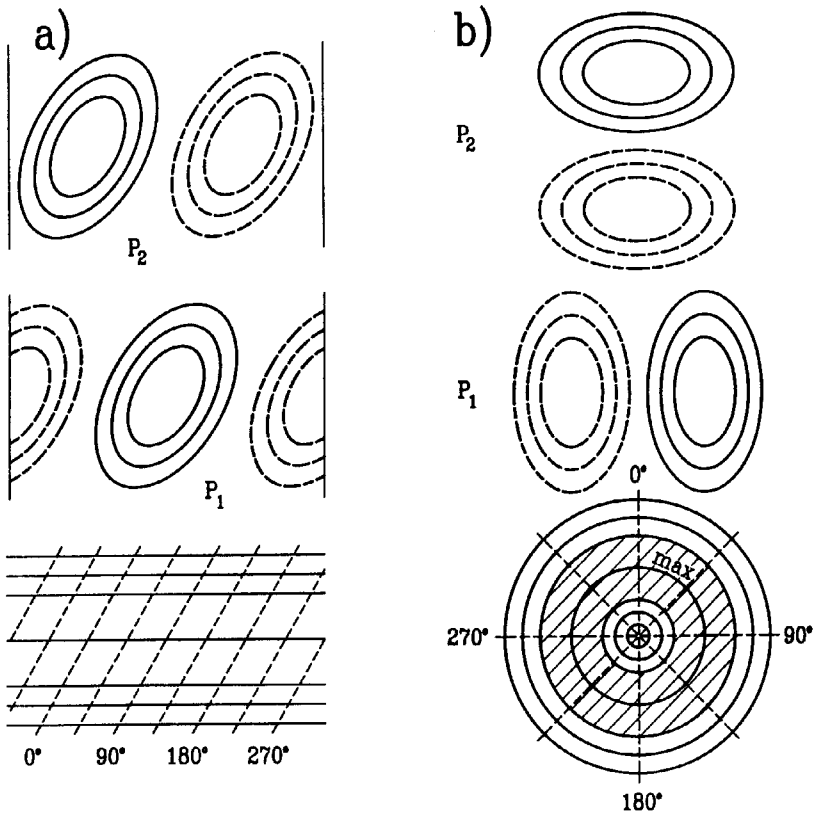

Figure 2. Examples of (a) a propagating wave and (b) an amphidromal wave and their representation in terms of POPs. Top two panels: representation by $\mathbf{p}^1$ and $\mathbf{p}^2$. Bottom panel: representation by phase ψ (dashed) and amplitude A (solid). From von Storch et al. (1988).

Time coefficients. The pattern coefficients z_j are given as the dot product of $\mathbf{x}$ with the *adjoint patterns* $\mathbf{p}_j^A$, which are the normalized eigenvectors of $\mathcal{A}^T$:

$$(\mathbf{p}_j^A)^T \mathbf{x} = \sum_k z_k (\mathbf{p}_j^A)^T \mathbf{p}_k = z_j \tag{8}$$

POPs. All information used so far is the existence of a linear equation Eq. (1) with some matrix $\mathcal{A}$. No assumption was made about the origin of this matrix. In dynamical theory, the origins of Eq. (1) are linearized and discretized differential equations. In case of the POP analysis, the relationship

$$\mathbf{x}(t+1) = \mathcal{A} \cdot \mathbf{x}(t) + \text{noise} \tag{9}$$

is hypothesized. Multiplication of Eq. (9) from the right hand side by the transposed $\mathbf{x}^T(t)$ and taking expectations, E, leads to

$$\mathcal{A} = E[\mathbf{x}(t+1)\mathbf{x}^T(t)] \cdot \left[E[\mathbf{x}(t)\mathbf{x}^T(t)]\right]^{-1}. \tag{10}$$

The eigenvectors of Eq. (10) or the normal modes of Eq. (9) are called *principal oscillation patterns*. The coefficients z are called *POP coefficients*. Their time evolution is given by Eq. (3), superimposed by noise

$$z(t+1) = \lambda \cdot z(t) + \text{noise}. \tag{11}$$

The stationarity of Eq. (11) requires $\rho < 1$. In practical situations, when only a finite time series $\mathbf{x}(t)$ is available, $\mathcal{A}$ is estimated by first deriving the sample lag-1 covariance matrix $\mathcal{X}_1 = \sum_t \mathbf{x}(t+1)\mathbf{x}^T(t)$ and the sample covariance matrix $\mathcal{X}_0 = \sum_t \mathbf{x}(t)\mathbf{x}^T(t)$ and then forming $\mathcal{A} = \mathcal{X}_1\mathcal{X}_0^{-1}$. The eigenvalues of this matrix always satisfy $\rho < 1$.

To reduce the number of spatial degrees of freedom in some applications, the data are subjected to a truncated empirical orthogonal function (EOF) expansion, and the POP analysis is applied to the vector of the first EOF coefficients. A positive by-product of this procedure is that noisy components can be excluded from the analysis. Then, the covariance matrix $\mathcal{X}_0$ has a diagonal form.

If there is a priori information that the expected signal is located in a certain frequency band, it is often advisable to time-filter the data prior to the POP analysis. A somewhat milder form of focusing on selected time scales is to derive the EOFs from time-filtered data and then to project the unfiltered data on these EOFs.

Criteria to decide whether a POP contains useful information or if it should be regarded as reflecting mostly sample properties are given by von Storch et al. (1988). The most important rule-of-thumb is related to the cross spectrum of the POP coefficients z^1 and z^2: at the POP period T, or at least in the neighborhood of T, the two time series should be significantly coherent and 90° out of phase, according to Eq. (6).

Invariance against coordinate transformations. If the original time series $\mathbf{x}(t)$ is transformed into another time series $\mathbf{y}(t)$ by means of $\mathbf{y}(t) = \mathcal{L} \cdot \mathbf{x}(t)$ with an invertible matrix $\mathcal{L}$, (i.e., $\mathcal{L}^{-1}$ exists), then the eigenvalues are unchanged and the eigenvectors transform as x:

$$\mathcal{A}_X = \mathcal{X}_1\mathcal{X}_0^{-1}; \mathcal{A}_Y = \mathcal{Y}_1\mathcal{Y}_0^{-1}$$

with $\mathcal{Y}_1 = E(\mathbf{y}(t+1)\mathbf{y}^T(t)) = \mathcal{L}\mathcal{X}_1\mathcal{L}^T$ and $\mathcal{Y}_0 = \mathcal{L}\mathcal{X}_0\mathcal{L}^T$. Thus $\mathcal{A}_Y = \mathcal{L}\mathcal{A}_X\mathcal{L}^{-1}$. If $\mathbf{p}_X$ is an eigenvector of $\mathcal{A}_X$ with eigenvalue λ, i.e., $\mathcal{A}_X\mathbf{p}_X = \lambda\mathbf{p}_X$ then $\mathcal{A}_X\mathcal{L}^{-1}\mathcal{L}\mathbf{p}_X = \lambda\mathbf{p}_X$ and, eventually $\mathcal{L}\mathcal{A}_X\mathcal{L}^{-1}(\mathcal{L}\mathbf{p}_X) = \lambda(\mathcal{L}\mathbf{p}_X)$. That is, if $\mathbf{p}_X$ is a POP of the time series **x**, then $\mathcal{L}\mathbf{p}_X = \mathbf{p}_Y$ is a POP of **y** with the same eigenvalue λ.

The EOFs are *not* invariant against linear transformations $\mathcal{L}$, since in general the matrices $\mathcal{X}_0$ and $\mathcal{L}\mathcal{X}_0\mathcal{L}^T$ will have different eigenvalues and eigenvectors. Therefore, if the POP analysis is begun with a projection of the data on a truncated EOF expansion, the results of a POP analysis will change if the data are transformed into another coordinate system.

The POP coefficients. To get the POP coefficients, $z(t)$, two approaches are possible. One is to derive the adjoint patterns $\mathbf{p}^A$ and to use Eq. (8). An alternative is to not derive adjoint patterns but to derive the coefficients z by a least-square fit of the data **x** by minimizing

$$\left\|\mathbf{x} - z\cdot\mathbf{p} - \left[z\cdot\mathbf{p}\right]^*\right\| = \left\|\mathbf{x} - z^1\mathbf{p}^1 - z^2\mathbf{p}^2\right\| \tag{12}$$

if **p** is complex, or

$$\left\|\mathbf{x} - z\cdot\mathbf{p}\right\|. \tag{13}$$

2.2 POPs = Trivial Case of PIPs

State space models. Many complex dynamical systems, $\mathbf{x} \in R^n$, may conveniently be approximated as being driven by a simpler dynamical system, $\mathbf{z} \in R^m$, with a reduced number of degrees of freedom, $m \le n$. Mathematically, this may be described by a *state space model* which consists of a *system* equation

$$\mathbf{z}(t+1) = \mathcal{F}\left[\mathbf{z}(t), \alpha, t\right] + \text{noise}, \tag{14}$$

for the dynamical variables $\mathbf{z} = (z_1, \ldots, z_m)$ and an *observation* equation

$$\mathbf{x}(t) = \mathcal{P}\,\mathbf{z}(t) + \text{noise} = \sum_j z_j(t)\mathbf{p}_j + \text{noise} \tag{15}$$

for the observed variables **x**. $\mathcal{P}$ is the matrix whose columns are the vectors, or *patterns*, $\mathbf{p}_j$. In general $\mathcal{P}$ is not a square-matrix. $\mathcal{F}\left[\mathbf{z}(t), \alpha, t\right]$ denotes a class of models which can be nonlinear in the dynamical variables **z** and which depends additionally on a set of free parameters $\alpha = (\alpha_1, \alpha_2, \ldots)$. Both equations, Eqs. (14,15), are disturbed by an additive noise.

Since $m \leq n$, the time coefficient $z_j(t)$ of a pattern $\mathbf{p}_j$ at a time t is not uniquely determined by the $\mathbf{x}(t)$. Instead, it may be obtained by a least-square fit, i.e.,

$$\mathbf{z}(t) = (\mathcal{P}^T\mathcal{P})^{-1}\mathcal{P}^T\mathbf{x}(t). \tag{16}$$

The intriguing aspect of state space models is that the dynamical behavior of complex systems often appears to be dominated by the interaction of only a few characteristic patterns $\mathbf{p}_j$. That is, even if the dynamics of the full system are restricted to the subspace spanned by the columns of $\mathcal{P}$, its principal dynamical properties are represented.

PIPs. When fitting the state space model Eqs. (14,15) to a time series, the following entities have to be specified: the class of models $\mathcal{F}$, the patterns $\mathcal{P}$, the free parameters α, and the dimension of the reduced system m. The class of models $\mathcal{F}$ has to be selected a priori on the basis of physical reasoning. Also, the number m might be specified a priori. The parameters α and the patterns $\mathcal{P}$ are fitted simultaneously to a time series by requesting them to minimize

$$\epsilon[\mathcal{P};\alpha] = \mathrm{E}\left\| \mathbf{x}(t+1) - \mathbf{x}(t) - \mathcal{P}(\mathcal{F}[\mathbf{z}(t),\alpha,t] - \mathbf{z}(t))\right\|^2 \tag{17}$$

where $\epsilon[\mathcal{P};\alpha]$ is the mean square error of the approximation of the (discretized) time derivative of the observations $\mathbf{x}$ by the state space model. The patterns $\mathcal{P}$, which minimize Eq. (17), are called *principal interaction patterns* (Hasselmann, 1988). If only a finite time series of observations $\mathbf{x}$ is available, the expectation E is replaced by a summation over time.

In general, the minimization of Eq. (17) is not unique. In particular, the set of patterns $\mathcal{P}' = \mathcal{P} \cdot \mathcal{L}$ with any nonsingular squared matrix $\mathcal{L}$ will minimize Eq. (17), if $\mathcal{P}$ does, as long as the corresponding model $\mathcal{F}' = \mathcal{L}^{-1}\mathcal{F}$ belongs to the a priori specified model class. This problem may be solved by requesting the solution to fulfill some constraints, e.g., that the linear term in the Taylor expansion of $\mathcal{F}$ is a diagonal matrix.

POPs as PIPs. The principal oscillation patterns can be understood as a kind of simplified principal interaction patterns. For that assume $m = n$. Then, the patterns $\mathcal{P}$ span the full $\mathbf{x}$-space, and their choice does not affect $\epsilon[\mathcal{P};\alpha]$. Also, let $\mathcal{F}$ be a linear model $\mathcal{F}[\mathbf{z}(t),\alpha] = \mathcal{A} \cdot \mathbf{z}(t)$, where the parameters α are the entries of $\mathcal{A}$. Then the dynamical equation Eq. (14) is identical to Eq. (11). The constraint mentioned above leads to the eigenvectors of $\mathcal{A}$ as being the PIPs of the particular, admittedly simplified, state space model.

2.3 Associated Correlation Patterns

Definition and representation. The *associated correlation pattern analysis* (von Storch et al., 1988) is a regression analysis to infer the spatial properties of a signal which is encoded in a two-dimensional index (a complex POP coefficient, for instance). If the parameter under consideration is $\vec{\mathbf{Y}}(t)$ and the bivariate index is $(z^1(t), z^2(t))$ the two associated correlation patterns $\vec{q}^1$ and $\vec{q}^2$ minimize

$$\sum_t \left\| \vec{\mathbf{Y}}(t) - \frac{z^1(t)}{\sqrt{2}}\vec{q}^1 - \frac{z^2(t)}{\sqrt{2}}\vec{q}^2 \right\|^2 = \min. \tag{18}$$

The normalization with $\sqrt{2}$ in Eq. (18) has been introduced so that $\vec{q}^1$ represents a typical state for $z^1(t) = 1$, $z^2(t) = 0$ and $\vec{q}^2$ a typical state for $z^1(t) = 0$, $z^2(t) = 1$. The solution of Eq. (18) is straightforward and requires the solution of a 2×2 linear equation at each location r of the input field $\vec{\mathbf{Y}} = (\mathbf{y}_r)$.

The associated correlation patterns can be displayed directly by the two patterns $\vec{q}^1$ and $\vec{q}^2$ or by amplitude distributions and phase distributions (Figure 6). The amplitude A and the phase ψ at the location r is given by

$$A = \sqrt{(\vec{q}^1)^2 + (\vec{q}^2)^2} \tag{19}$$

$$\tan\left(2\pi\frac{\psi}{T}\right) = \frac{-\vec{q}^2}{\vec{q}^1} \tag{20}$$

with T being the period of the mode. The phase ψ has been defined such that $\psi = 0$ coincides with $z^2 = 0$ and $z^1 > 0$, and $\psi = T/4$ with $z^1 = 0$ and $z^2 < 0$ (compare with Eq. (7)).

Measure of skill. A number measuring the relative importance of a POP for a parameter $\mathbf{y}_r$ at the location r is the rate of explained $\mathbf{y}_r$-variance by the index (z^1, z^2). This rate is given by

$$\varepsilon(\mathbf{y}_r, z^1, z^2) = \frac{\mathrm{Var}(\mathbf{y}_r) - \epsilon_r^2}{\mathrm{Var}(\mathbf{y}_r)} \tag{21}$$

with

$$\epsilon_r^2 = \sum_t \left[\mathbf{y}_r(t) - \frac{z^1(t)}{\sqrt{2}\,\sigma_1}\vec{q}_r^1 - \frac{z^2(t)}{\sqrt{2}\,\sigma_2}\vec{q}_r^2 \right]$$

being the local error in Eq. (18); $\varepsilon = 1$ indicates a perfect model and $\varepsilon = 0$ a model without skill.

3. POP ANALYSIS OF THE INTRASEASONAL VARIABILITY IN THE EQUATORIAL PACIFIC

General. The general analysis strategy is first to derive an index of the equatorial modes through a principal oscillation pattern (POP) analysis of the equatorial current meter moorings at 165°E, 140°W, and 110°W. The time series at these stations are relatively long and sample the equator fairly well. Zonal currents and temperatures, which ought to reflect equatorial Kelvin waves well, as well as meridional currents are monitored by these buoys. After having established that the index makes sense, all available data from the current meter moorings and from the ATLAS buoys are examined in an "associated correlation pattern" analysis. The purpose of this exercise is to infer the 3-dimensional spatial structure of the modes.

3.1 Raw Data

For the analysis, daily observations were available from two series of moored buoys (Hayes et al., 1991):

- Current meter moorings at four locations, the exact positions of which are given in Table 1. These buoys recorded zonal and meridional currents and temperature at various levels and near surface air temperature and zonal and meridional wind.

- ATLAS buoys located at 20 positions in the near-equatorial Pacific (for the exact positions, see Table 1). From these buoys, subsurface temperatures at various levels, as well as near surface air temperature and wind, are available.

The shortest time series is from 147°E, 5°N (9 months). Maximum length is 7 years (at 0°, 110°W and 140°W).

Mean State. The buoy data represent a good data base to sketch the mean distribution of currents and temperature in the equatorial Pacific. In Figure 3 are plotted the mean zonal current and temperature distributions along the equator as well as latitude-depth cross-sections of temperature along 165°E and 110°W. The mean equatorial temperature distribution is dominated by the sharp thermocline that separates water of 10–15°C at deeper layers from warm surface waters of 24°C in the east and 28°C in the west. If we identify the thermocline with the 20°C isotherm, then the thermocline rises from 180 m at

165°E to 100 m at 140°W to 60 m at 110°W. The zonal current is weakly westward at the surface with maximum values below 25 cm/s. Maximum eastward flowing currents, the *Equatorial Undercurrent*, prevail along the thermocline, with maximum values at about the 17.5°C isotherm. At 165°E the maximum current is below 50 cm/s, at 140°W maximum speeds are 100 cm/s, and at 110°W above 75 cm/s.

Maximum temperatures prevail north of the Equator in the east and south of the Equator in the west. The thermal wind relationship is nicely reflected in the mean distributions (Fig. 3a, c and d).

Table 1. Position of buoys from which data have been used in the present study. Also given is the maximum time interval for which at least one variable is available.

Instrument	Longitude	Latitude	Data interval	Parameters
CMM	0°	165°E	5/86 - 4/91	current, temperature, wind
CMM	0°	140°W	5/84 - 4/91	
CMM	0°	110°W	5/84 - 4/91	
CMM	7°N	110°W	5/88 - 4/91	
ATLAS	5°N	147°E	5/90 - 2/91	temperature, wind
ATLAS	8°N	165°E	5/90 - 4/91	
ATLAS	5°N	165°E	7/88 - 4/91	
ATLAS	2°N	165°E	7/87 - 4/91	
ATLAS	2°S	165°E	5/86 - 4/91	
ATLAS	5°S	165°E	7/87 - 4/91	
ATLAS	0°	169°W	5/88 - 4/91	
ATLAS	7°N	147°W	11/88 - 11/90	
ATLAS	9°N	140°W	5/88 - 4/91	
ATLAS	5°N	140°W	5/88 - 4/91	
ATLAS	2°N	140°W	5/87 - 4/91	
ATLAS	2°S	140°W	5/87 - 4/91	
ATLAS	5°S	140°W	10/90 - 4/91	
ATLAS	7°N	132°W	5/89 - 10/90	
ATLAS	0°	124°W	5/87 - 4/91	
ATLAS	5°N	110°W	5/86 - 4/91	
ATLAS	2°N	110°W	6/85 - 4/91	
ATLAS	2°S	110°W	5/85 - 4/91	
ATLAS	5°S	110°W	5/86 - 4/91	
ATLAS	8°S	110°W	5/86 - 6/87	

Variability around the annual cycle. The annual cycles have been removed from all data. To also exclude part of the Southern Oscillation-related variability, this removal of

the annual cycle was done for each May-to-April segment separately. The May-to-April segments were chosen to represent one "El Niño year" (Wright ,1985). As an example, three variables at 0°, 140°W are shown before and after the removal of the low-frequency variability (Figure 4).

At the equatorial buoy all parameters undergo marked variations on the interannual time-scale, some of which stem mostly from the regular annual cycle (e.g., the zonal wind). In the subsurface variables the irregular ENSO-related variations contribute most to the low frequency variability. The high-frequency variations are normally distributed. In the zonal wind the intraseasonal variations are almost white in time, whereas the subsurface parameters exhibit an oscillatory behavior with typical periods of 50–100 days. The zonal current seems to lead the temperature by a few days.

3.2 The POP Analysis of the Equatorial Current Meter Mooring Data

Preprocessing of the data. In the data field to be analysed, we have parameters that differ with respect to units as well with respect to their standard deviations. To allow all parameters to play the same role in the analysis, all data are standardized to zero mean and standard deviation one.

For the POP analysis it is often helpful if the data are preprocessed prior to the analysis with the purpose of suppressing space-time noise (see section 2.1). The spatial noise is taken out by doing the analysis in a low-dimensional subspace spanned by the first few EOFs, and the temporal variations on time scales irrelevant for the process under investigation are taken out by a time filter.

The data are first subjected to an EOF analysis. In this EOF analysis the entries γ_{ij} of the correlation matrix have been estimated from all available pairs of observations, i.e.,

$$\gamma_i = \frac{1}{n_{ij}} \sum_{t \in \mathcal{T}_{ij}} p_i(t) p_j(t) \tag{22}$$

where $p_i(t)$ represents the i-parameter of the data field $\vec{\mathbf{X}}(t)$ at time t. $\mathcal{T}_{ij}$ is the set of all times when both p_i and p_j have been observed and n_{ij} is the number of elements in $\mathcal{T}_{ij}$ Definition Eq. (22) is adequate for the case of gappy data. Only those pairs of indices (i,j) were considered for which n_{ij} was at least 50% of all possible observations.

The EOF coefficients $\alpha^k(t)$ are then no longer given as the dot product of the field $\vec{\mathbf{X}}(t)$ at time t and the respective EOF $\vec{e}^k$ but are determined as a least-square-fit

$$\left\| \vec{\mathbf{X}}(t) - \alpha^k(t) \times \vec{e}^k \right\| = \min. \tag{23}$$

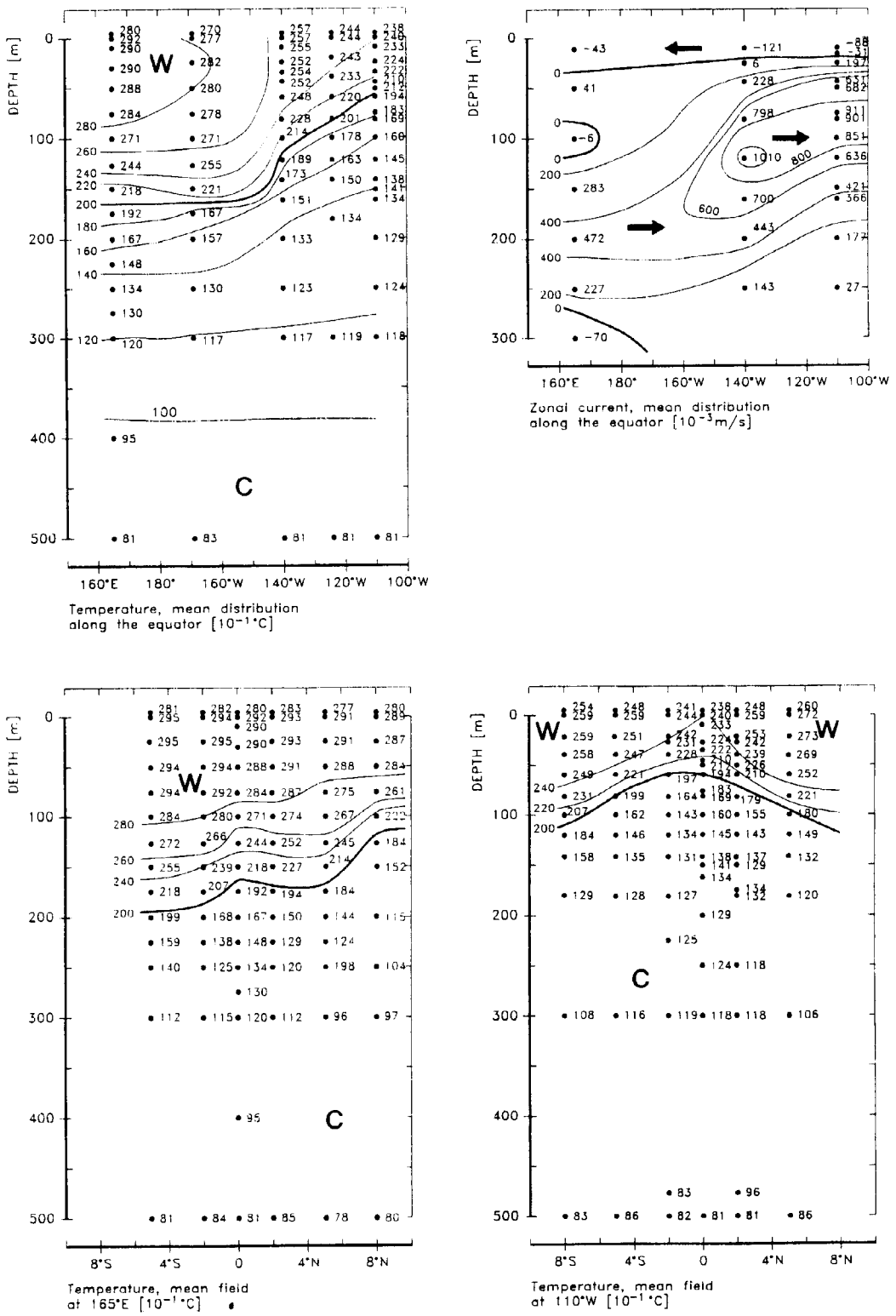

Figure 3. Mean distributions derived from the buoy data. The 20°C isotherm in the temperature distributions (in 10^{-1} °C) and the zero line in the current distribution (in 10^{-3} m/s) are given as heavy lines. Top: Longitude-depth cross sections of temperature and zonal current along the equator. Bottom: Latitude-depth cross-sections of temperature along 165°E and 110°W.

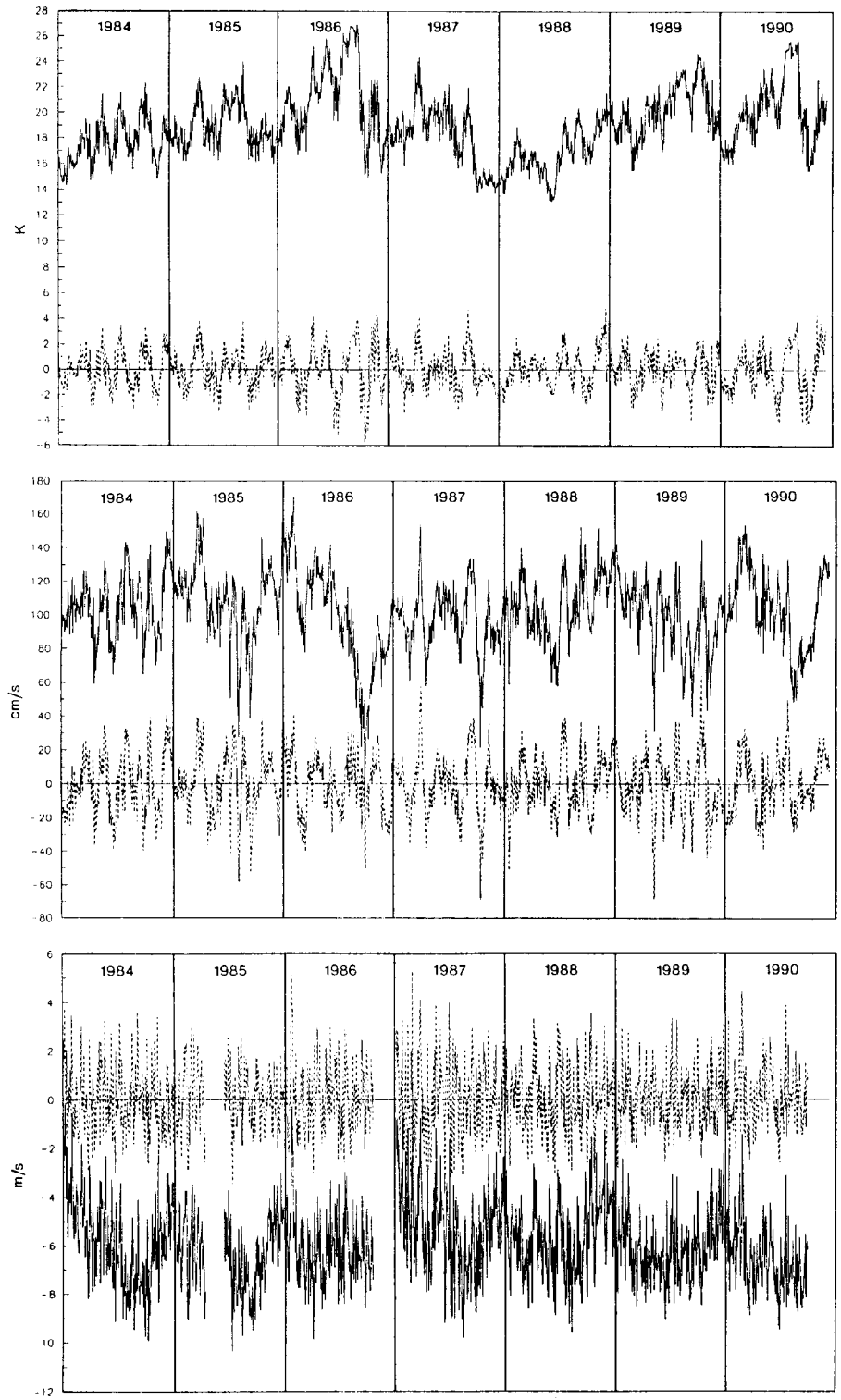

Figure 4. Time series at 0°, 140°W for temperature and currents at 120 m and for zonal wind, before and after subtraction of the annual cycle and of low-frequency variations. The years are given as May-to-April segments.

The EOF coefficients $\alpha^k(t)$ represent complete time series over the entire 7-year time interval from May 1984 through April 1991. These time series are time-filtered such that all variability below 10 days and above 180 days is completely eliminated and all variability on time scales between 40 and 150 days is not affected. In the windows between 10 and 40 days and 150 and 180 days the filter response function smoothly changes from 0 to 1.

Results of POP analysis. Two oscillatory modes are identified whose coefficient time series exhibit the desired high coherency and 90°-out-of-phase relationship. In Figure 5 the amplitude time series of the two complex POP coefficients are plotted. Note that the coefficient time series have been normalized so that $\mathrm{Var}(z^i(t)) = 1$. The coefficients were obtained by means of the adjoint patterns and Eq. (8).

One mode has a POP period $T = 65$ days, and an e-folding time $\tau = 73$ days. It represents about 16% of the variance of the band-pass filtered, EOF-truncated and normalized data (at all three locations, for temperature, zonal, and meridional currents as well as winds, and at all depths). In consistency with the POP period the maximum coherence is obtained for 60 days. The amplitude time series reveals a marked annual cycle, with a definite appearance of a semiannual component. The wave activity is strongest during solstice conditions and minimum activity during equinoctial conditions.

The second mode has an e-folding time of 106 days and a POP period $T = 120$ days. But the POP coefficients $z^1(t)$ and $z^2(t)$ have largest coherencies at 72 days, so that the POP period of 120 days likely is an overestimate of the true oscillation period. The POP coefficient represents 18% of the variance of the band-pass filtered, EOF-truncated, and normalized data. The amplitude time series in Figure 5 are hardly affected by the annual cycle. Instead the modification of the large-scale environment through the development of warm El Niño conditions leaves a clear mark on the time series. During the warm event in 1986/87 and the early phase of the warm event in 1990/91 the activity of the waves is enhanced.

The two modes are only weakly correlated. The correlations between the real and imaginary parts of the coefficient time series are very small, and the correlations between the real (imaginary) parts of the two modes are about –0.25.

3.3 The Spatial Signature of the Mode

General. In the present study, associated correlation patterns have been computed from various parameters for both modes separately. In all cases the annual cycle, as represented by the first two annual harmonics and the overall mean of each May-to-April segment, has been removed prior to the analysis. No more time-smoothing was done because of the wide gaps in the data. An implicit time-filtering has been introduced through the use of the

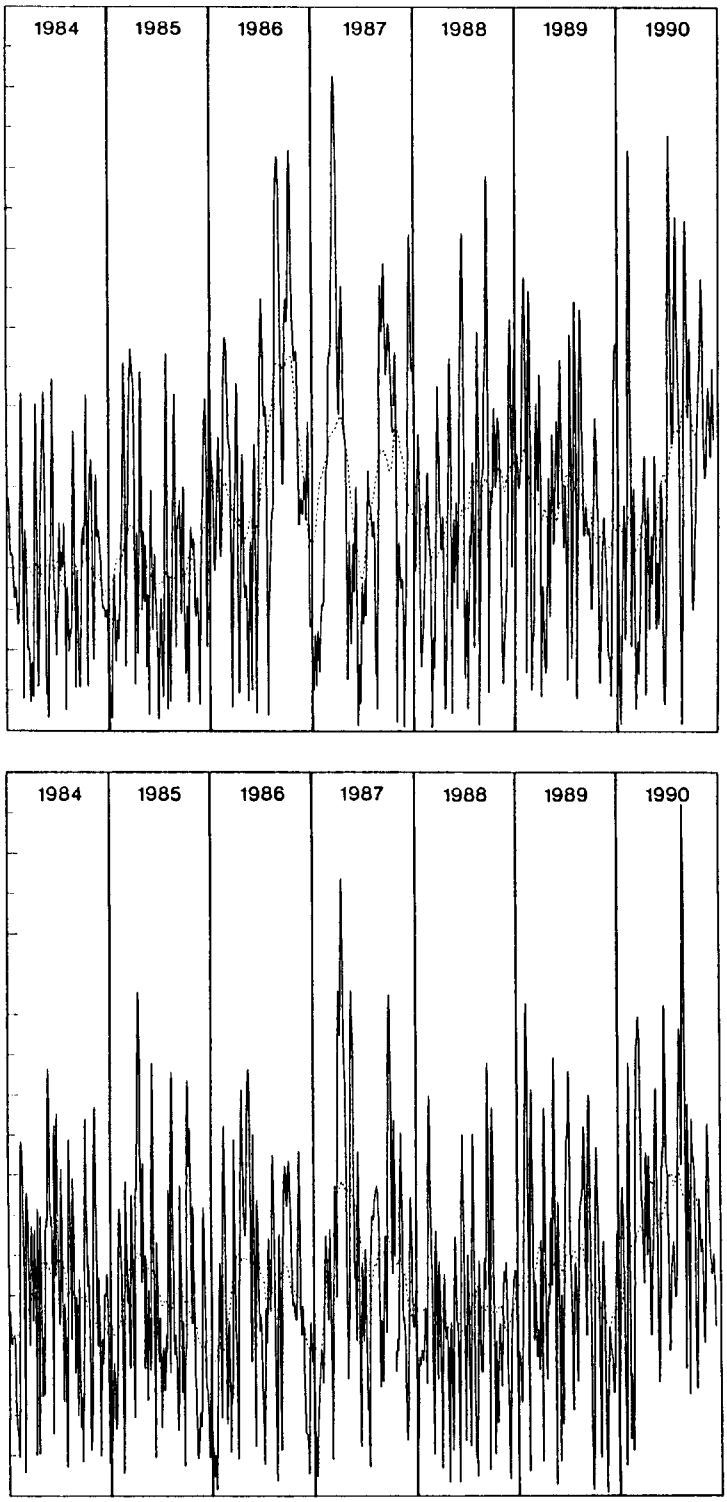

Figure 5. Time series of the amplitude of the two modes identified in the joint POP analysis of normalized data from equatorial current meter moorings. The years are drawn as May-to-April segments. (a) The 120 day mode. (b) The 65 day mode.

POP coefficient time series. Since these time series have been derived from time-filtered data (see above), they are themselves smooth. Unlike the POP analysis, the data are not normalized for the associated correlation pattern analysis.

Currents at the current meter moorings. The longitude-depth distributions of the amplitudes and phases of the two intraseasonal modes, with POP periods of 120 days and 65 days, are shown in Figure 6 for the zonal current. Both modes represent eastward propagating signals.

The 120-day mode has its largest amplitudes in the central part of the tropical Pacific, with maximum values of 16 cm/s, as typical anomalies, at 50 m depth at 165°E and 160 m depth at 140°W. In contrast, the 65-day mode has maximum zonal current anomalies at upper levels (50 m and above) in the eastern part of the basin, with a typical maximum of 12 cm/s at 140°W and 19 cm/s at 110°W.

In the 120-day mode, the zonal current signals need about 60 days to propagate from the 165°E buoy to the easternmost buoy at 110°W. If we accept the estimate of 120 days as a period, then the mean phase speed is 1.8 m/s. This number is increased to 2.4 m/s or 3.0 m/s if the period is set to 90 or even 72 days (see above). The phase lines are vertically tilted at 165°E and 140°W, with the upper levels lagging the lower levels by about 45° or 15 days (of a 120-day period).

The phase speed for the 65-day mode is estimated to be, on an average, 2.1 m/s. At the two eastern positions, the phase lines are again tilted, with the lower levels leading the upper levels by about 45° or 8 days (of a 65-day period). Maximum explained local variance of the zonal current field is 40% at 120 m at 140°W for the 120-day mode and 20% at 120 m at 110°W for the 65-day mode.

Current information is also available for one off-equatorial location from the 7°N, 140°W buoy. Here a maximum of 7% of explained variance is obtained for the 120-day mode at 40 m, where an amplitude of 5.4 cm/s is found (not shown). Thus the signal is weak at that location, but interestingly the sign at 7°N is opposite to that at the equator (not shown). A similar result is found for the 65-day mode.

In the meridional current the signal is negligible for the 120-day mode, but a well-defined signal is identified in the 65-day mode. Maximum percentages of explained local variance are 12% at 120 m and 160 m at 110°W. A maximum amplitude of 10 cm/s near the surface lags an amplitude of about 8 cm/s at lower levels by about 10 days (not shown). The phase relationship with the zonal current is that northward meridional current anomalies lead easterly zonal current anomalies by 10 days or so. An alternative interpretation is that easterly current anomalies lead southward current anomalies by 20 days or so.

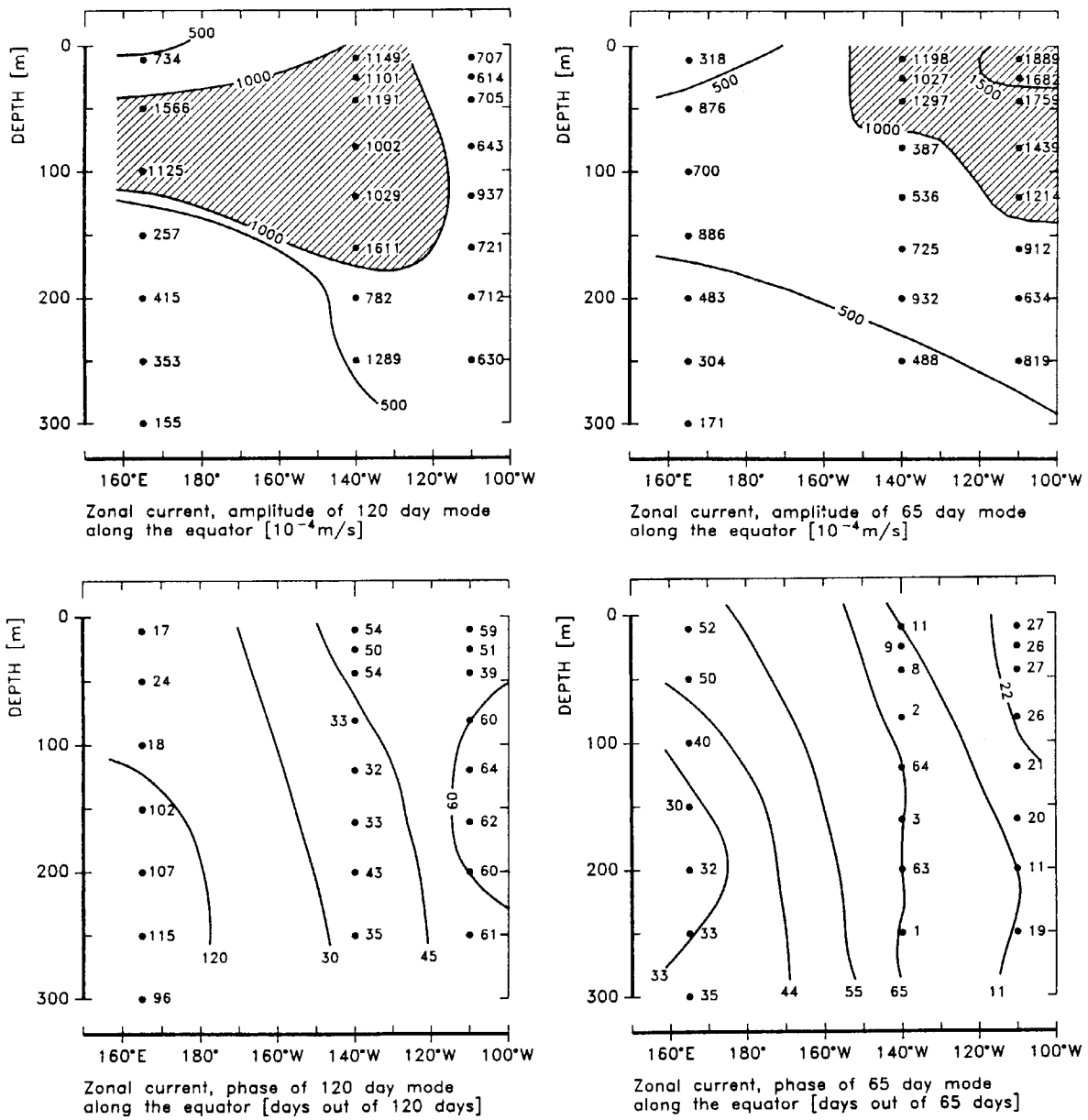

Figure 6. Longitude–depth cross-section of the zonal currents of the 120-day and 65-day mode along the equator. Top: The amplitudes A in 10^{-2} cm/s, and Bottom: The phases ψ in days (relative to base periods of 120 or 65 days).

Temperature at all buoys. For temperature, the amplitude distributions A and phase distributions ψ are shown as three cross sections through the tropical Pacific: a longitude-depth cross section along the equator (Fig. 7), a latitude-depth cross section at 110°W (Fig. 8), and a longitude-latitude cross section at 100 m (Fig. 9).

Maximum temperature amplitudes of both modes cluster along the thermocline (Fig. 3a) with maximum values of more than 1°C (Fig. 7). Overall, the temperature signal of the 120-day mode is stronger than that of the 65-day mode. The temperature signals propagate like the zonal current signals eastward along the equator. The 120-day temperature signal travels over the basin in about 90 days (relative to a base period of 120 days) so that the phase speed of temperature is 1.5 times that of the zonal current. At the 165°E buoy, the temperature and zonal current signals are almost in phase so that the later phase lags must stem from different travel times. The propagation of the temperature signal of the 65-day mode is mostly parallel to that of the zonal current signal but there is a uniform lag of about 10 days.

The latitude-depth cross sections of the associated correlation patterns at 110°W reveal maximum amplitudes of more than 1°C at about 100 m depth. In both modes are a marked amplitude minimum at 2°N and a maximum at 6°N. The activity of the 120-day mode is largest south of the equator, with a maximum amplitude of 1.4°C at 2°S, whereas the 65-day mode has its largest amplitude of 1.4°C at 6°N. Both modes exhibit complicated phase distributions. In the 120-day mode the phase varies mostly between 60 days at deeper levels and 90 days at upper levels. Only along the minimum at 2°N the phase is markedly lagging its neighborhood by 30 or more days. In the 65-day mode the maximum at 6°N is 180° out of phase with the temperature signal at the equator which, in turn, lags the secondary maximum at 2°S by another 10 to 15 days.

Figure 9 shows the latitude-longitude distributions of the amplitudes and phases of the two modes in 100 m depth. Maximum amplitudes of the order of 1°C at 140°W at the equator, where the thermocline is close to 100 m, tend to appear simultaneously with even larger (≈2°C) anomalies with opposite sign at 7°N. The eastward propagation is clearly visible in the 65-day mode, whereas in the 120-day mode the eastward propagation seems to be limited to the area west of 140°W. The isolated amplitude maximum at 5°N, 147°E should not be taken too seriously because of the shortness of the time series at that location (see Table 1).

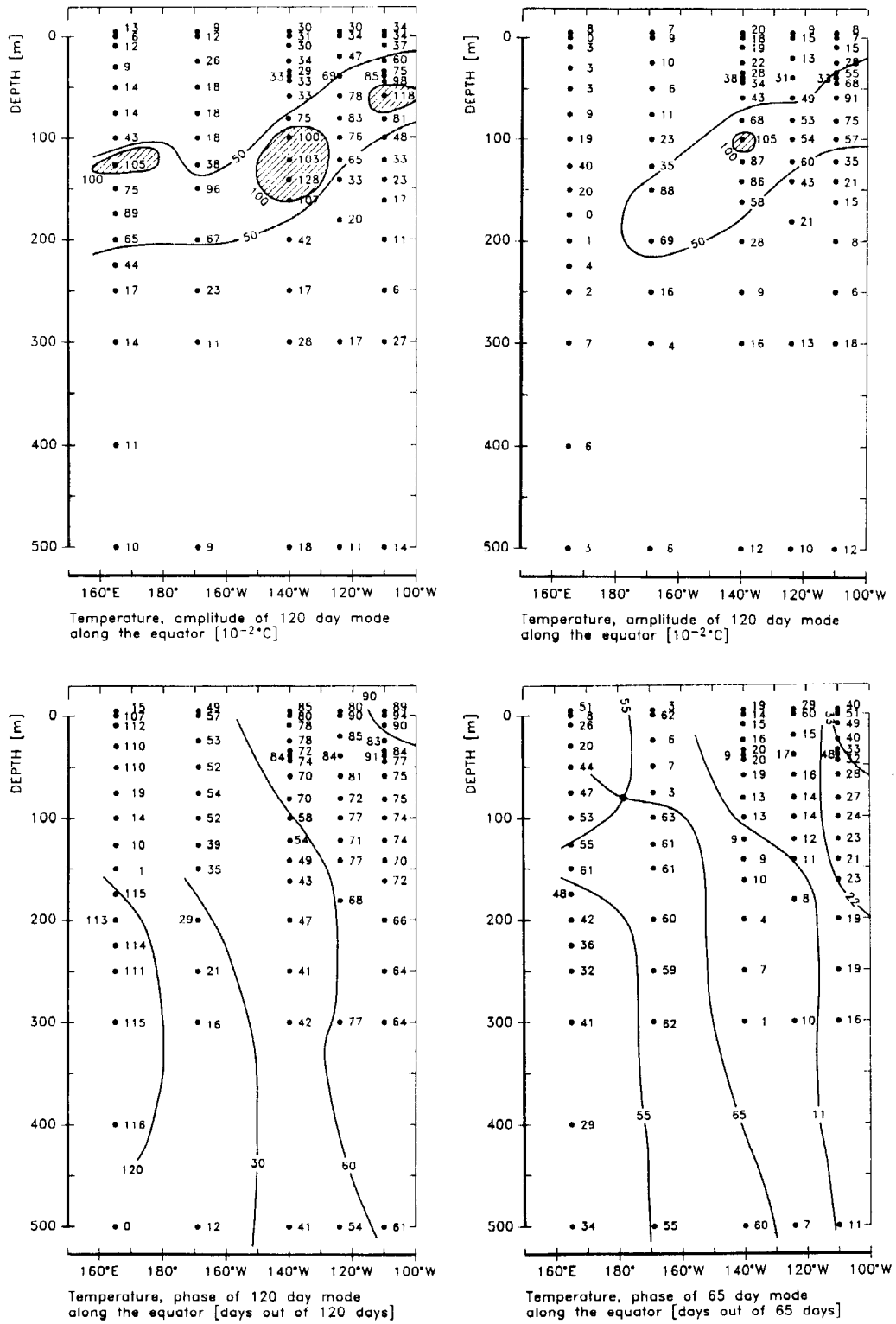

Figure 7. Longitude–depth cross-section of temperature of the 65 day mode and of 120 day mode along the equator. Top: The amplitude distributions A in 10^{-2} °C. Bottom: The phase distributions ψ (in days relative to the base periods of 120 and 65 days).

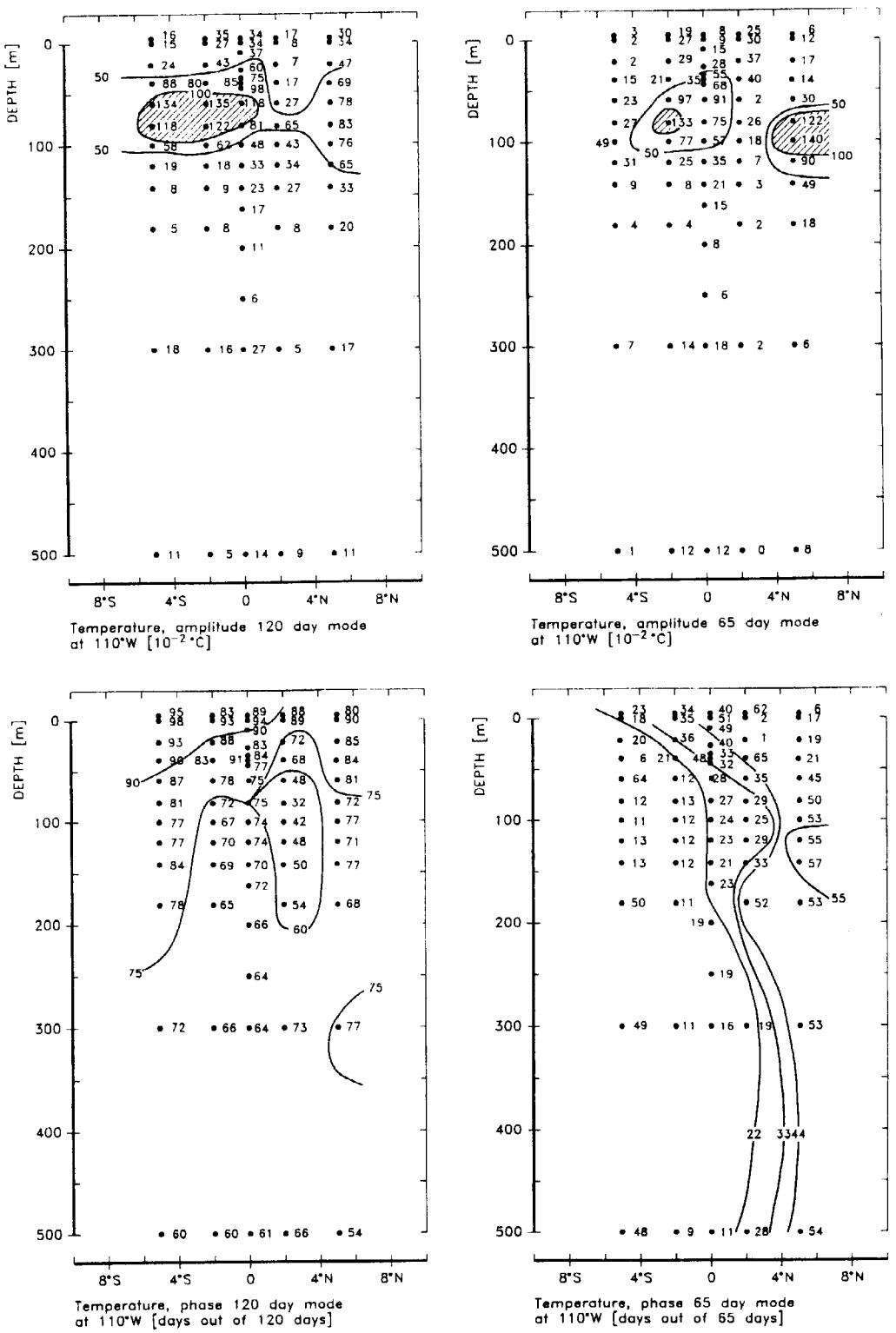

Figure 8. Latitude-depth distributions of temperature at 110°W and 140°W of the 120 day mode and of the 65 day mode. Top: Amplitude distributions A at 110°W (in 10^{-2} °C). Bottom: Phase distributions ψ at 110 °W (in days relative to the 120 day and 65 day base periods).

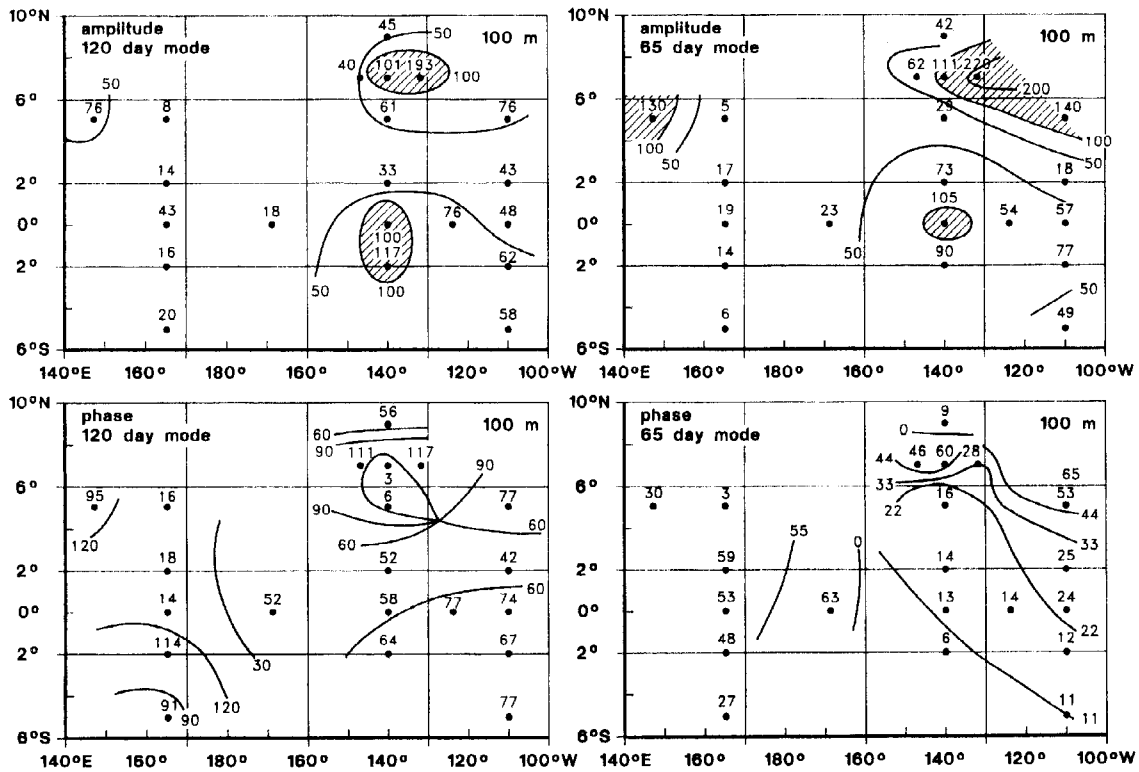

Figure 9. Horizontal distribution of temperature at a depth of 100 m of the 120 day mode and of the 65 day mode. Top: Amplitude distributions A in 10^{-2} °C. Bottom: Phase distributions ψ (in days relative to the 120 day and 65 day base periods).

Discussion: Equatorial temperature anomalies and advection. Because of the marked spatial gradients in the mean temperature field (Fig. 3) the temperature advection with the anomalous zonal currents might contribute significantly to the creation of temperature anomalies. Estimates of such temperature anomalies may be obtained for the equator since information on the currents is available there. If the anomalies are labelled by a * and the mean state by a $^{-}$, then the effect of the anomalous currents on the temperature is approximated by

$$\mathbf{T}^* \approx \left[\mathbf{u}^* \frac{\partial \overline{\mathbf{T}}}{\partial x} + \mathbf{v}^* \frac{\partial \overline{\mathbf{T}}}{\partial y} \right] \times \frac{T}{2} \tag{24}$$

with $\mathbf{T}$, $\mathbf{u}$, and $\mathbf{v}$ representing the temperature and zonal and meridional currents, and T the period; x refers to the zonal direction and y to the meridional direction. In the following we consider the situation at 140°W at 120 m depth.

The zonal gradient of the mean $\overline{\mathbf{T}}$ is approximately 2×10^{-8} K/cm (Fig. 3). For the 120 day mode the anomalous zonal current is 10 cm/s (Fig. 6) and the period is somewhere

between 80 to 120 days. Equation (24) yields with these numbers a temperature anomaly between 0.6 and 1.0°C, which compares well with the result of 1.0°C in Fig. 7. The 120 day mode is not connected with significant anomalies of the meridional current. Thus this back-of-the-envelope calculation Eq. (24) proposes that the equatorial temperature anomalies are due to anomalous zonal advection. This hypothesis is supported by the different travel times of the temperature and zonal current signal, which was found in a numerical experiment on the the response of the tropical Pacific to westerly wind bursts (Latif et al., 1988).

The typical zonal current anomalies of the 65 day mode are only 5.4 cm/s at 120 m (Fig. 6) and the characteristic time $T/2$ is only 32 days. Thus the effect of zonal advection is estimated as 0.3°C, which is significantly less than the predicted 0.9°C (Fig. 7). Thus zonal advection cannot fully explain the observed temperature anomalies—which is consistent with the coincidence of the temperature and zonal current travel times. The 65-day mode exhibits, however, a significant signal in the meridional current which could account for equatorial temperature anomalies of 0.3°C.

Kelvin waves? Are the modes identified and described so far what people call *Kelvin waves* (Moore and Philander, 1977)? The vertical structure of the modes along the equator, the horizontal scale, the eastward propagation and the time scale are broadly consistent with the concept of equatorial Kelvin waves. But several aspects are inconsistent with this concept. There are two modes, which have similar vertical structures, similar horizontal scales and time scales, that certainly cannot be accounted for as the first two Kelvin modes. The presence of a signal in the meridional signal in the 65 day mode does not fit the specification of a Kelvin wave nor has the rich structure found off the equator yet been described by the theory of equatorial Kelvin waves.

Johnson and McPhaden (1993) analyzed five years (1983-87) of current and temperature data from the 140°W and 110°W equatorial moorings and seven months of data from bouys at 2°S, 0° and at 2°N, 140°W. They used the complex empirical orthogonal functions (CEOFs, see also Section 4) and found one dominant mode that was broadly consistent with the idea of a first baroclinic Kelvin wave. The main differences from a conventionally defined Kelvin wave were these:

- A local maximum and a local minimum of the zonal velocity below and above the core of the equatorial undercurrent. This results holds for both modes identified in the POP analysis.
- An equatorial minimum of the temperature signal at the thermocline is straddled by two maxima at 2°S and 2°N. In the present POP analysis, on the other hand, the maximum at 2°S is reproduced, but north of the equator at 2°N a well-defined minimum is identified. Possibly Johnson and McPhaden's (1993) result is due to the short analysis period of only 210 days.

- A nonzero temperature signal at the surface lags the zonal current signal at the surface and the temperature signal at the thermocline by 90°. This result is confirmed by the POP analysis, in particular for the 120 day mode.

The biggest difference from Johnson and McPhaden (1993) is the presence of *two* modes which have uncorrelated coefficient time series but share substantial similarities in their spatial appearance. A reason for this difference might lie in the different analysis techniques. Johnson and McPhaden (1993) used CEOFs so that any two modes must be orthogonal in space whereas the POP analysis does not require orthogonality. If there are two orthogonal modes $(\mathbf{T}_i, \mathbf{u}_i)$ $(i = 1,2)$ with temperature signals **T** and zonal current signals **u** the orthogonality requires

$$\mathbf{T}_1^T \mathbf{T}_2 + \mathbf{u}_1^T \mathbf{u}_2 = 0. \tag{25}$$

Because of the sharp thermocline in the east equatorial Pacific the largest temperature anomalies will be centered around the thermocline so that $\mathbf{T}_1 \sim \mathbf{T}_2$. Thus to satisfy Eq. (25) a negative correlation of the current signals is needed, i.e., $\mathbf{u}_1 \sim -\mathbf{u}_2$. This latter condition represents a severe limitation without any physical justification. Therefore I speculate that the CEOF technique could not easily be used to identify two orthogonal modes in the equatorial **(T,u)** data. This (admittedly handwaving) argument might help to resolve the apparent contradiction of only one mode in Johnson and McPhaden (1993) but two modes in the POP analysis. On the other hand, there is no support in the literature (as far as I know) for the idea of two non-orthogonal modes.

The 65 day mode is not envisaged by the theory of equatorial wave dynamics. This theory deals with the growth of small disturbances and not with the development or breakdown of finite amplitude disturbances. Schnur et al. (1993) have shown, for the case of synoptic-scale disturbances in the extratropical troposphere, that the POP analysis is an adequate tool to obtain not only the normal modes of a dynamical system but also modes that represent finite amplitude phases in the full spectrum of variability. I speculate that the 65 day mode might represent such a finite amplitude mode. It remains to be clarified if the results of this study will stand the test of more data, longer time series, and closer scrutiny. However, one has also to keep in mind that the present theory of equatorial Kelvin waves is based on a number of severe simplifications, one being the horizontal homogeneity of the background state.

4. CONCLUSIONS

The purpose of the present paper is two-fold. The main point is to introduce the POP technique to the oceanographic community. The minor point is to present first results from an analysis of data that are irregularly distributed in space and time.

The POP technique. The POP method is a powerful method to infer simultaneously the space-time characteristics of a vector time series. The basic idea is to isolate low-dimensional subsystems that are controlled by the linear dynamics of the full system. Even if the POP method represents the most consistent way of doing so, there are other techniques that can be used successfully for similar purposes. An alternative is the *complex empirical orthogonal functions* (CEOFs; Wallace and Dickinson 1972, Barnett and Preisendorfer 1981). CEOFs are obtained by applying the conventional EOF technique to a complex time series whose real part is the real time series that has to be analysed and whose imaginary part is the Hilbert transform of that real time series. (CEOFs are related to EOFs just like complex POPs to regular POPs). The main difference between CEOFs and POPs is that CEOFs are constructed under the constraint of a maximum of explained variance and mutual orthogonality. The characteristic times, the period and the damping time, are not an immediate result of the CEOF analysis but have to be derived a posteriori from the CEOF coefficient time series. The POPs, on the other hand, are constructed to satisfy a dynamical equation Eq. (11), and the characteristic times are an output of the analysis; also the complex POP coefficients $z(t)$ are not pairwise orthogonal. The non-orthogonality makes the mathematics less elegant, but it is not a physical drawback, because in most cases there is no reason to assume that different geophysical processes develop statistically independent from each other. The rate of variance explained by the POPs is not optimal and has to be calculated after the POP analysis from the POP coefficients.

The POP method is not a tool that is useful in all applications. If the analysed vector time series exhibit a strongly non-linear behaviour, as in turbulent flows, the POPs will fail to identify a useful sub-system, simply because a linear sub-system does not control a significant portion of the variability. The POP method will be useful if there are a priori indications that the processes under consideration are to a first approximation linear.

Equatorial Waves. We have found two modes of variability in the equatorial Pacific Ocean. The slower mode, with a nominal period of 120 days, resembles a first baroclinic Kelvin wave. The other, 65-day mode is different from theoretically derived modes and from previously empirically derived modes. More work is needed to ensure the reality and the signature of the two distinct modes.

Acknowledgments. The present work was mostly done during a two-month visit to the Joint Institute for Marine and Atmospheric Research in Honolulu. I want to thank Dennis Moore, Peter Müller and Gary Mitchum, among others, for a scientifically stimulating visit. The buoy data have been made available by the Director of the TOGA-TAO Project Office, Dr. Michael J. McPhaden. The buoy data were prepared by Artur Urbanowicz at the MPI. Marion Grunert prepared the professionally drawn diagrams.

References

Barnett, T.P. and R. Preisendorfer, 1981, Origins and levels of monthly and seasonal forecast skill for United States surface air temperature determined by canonical correlation analysis. *Mon. Wea. Rev.* 115, 1825-1850.

Blumenthal, B., 1991, Predictability of a coupled ocean-atmosphere model. *J. Climate* 4, 766-784.

Bürger, G., 1993, Complex Principal Oscillation Patterns. *J. Climate* (in press).

Gallagher, F., H. von Storch, R. Schnur and G. Hannoschöck, 1991, The POP Manual. Deutsches Klimarechenzentrum, Bundesstrasse 55, 2000 Hamburg 13, Germany.

Hasselmann, K.H., 1988, PIPs and POPs: The Reduction of Complex Dynamical Systems Using Principal Interaction and Oscillation Patterns. *J. Geophys. Res.* 93, 11 015-11 021.

Hayes, S.P., L.J. Mangnum, J. Picaut, A. Sumi and K. Takeuchi, 1991, TOGA-TAO: A moored array for real time measurements in the Tropical Pacific Ocean. *Bull. Am. Met. Soc.* 72, 339-347.

Johnson, E.S. and M.J. McPhaden, 1993, On the structure of intraseasonal Kelvin waves in the Equatorial Pacific Ocean. *J. Phys. Oceanogr.* 23, 608-625.

Latif, M., J. Biercamp and H. von Storch, 1988, The response of a coupled ocean-atmosphere general circulation model to wind bursts. *J. Atmos. Sci.* 45, 964-979.

Latif, M. and, M. Flügel, 1990, An investigation of short range climate predictability in the tropical Pacific. *J. Geophys. Res.* 96, 2661-2673.

Latif, M., A. Sterl, E. Maier-Reimer and M.M. June, 1993, Climate variability in a coupled GCM. Part I: The tropical Pacific. *J. Climate* 6, 5-21.

Latif, M., and A. Villwock, 1989, Interannual variability in the tropical Pacific as simulated in coupled ocean-atmosphere models. *J. Marine Sys.* 1, 51-60.

Mikolajewicz, U. and E. Maier-Reimer 1991, One example of a natural mode of the ocean circulation in a stochastically forced ocean general circulation model. In: *Strategies for Future Climate Research* (Ed. M. Latif), 287-318, Max-Planck-Institut für Meteorologie Hamburg.

Moore, D. and G. Philander, 1977, Modelling of the tropical oceanic circulation. In: *The Sea* 6, 319-361, John Wiley and Sons Inc.

Schnur, R., G. Schmitz, N. Grieger and H. von Storch, 1993, Normal Modes of the atmosphere as estimated by principal oscillation patterns and derived from quasi-geostrophic theory. *J. Atmos. Sci.* (in press).

von Storch, H., T. Bruns, I. Fischer-Bruns and K. Hasselmann, 1988, Principal Oscillation Pattern analysis of the 30- to 60-day oscillation in a General Circulation Model equatorial troposphere. *J. Geophys. Res.* 93, 11 022-11 036.

von Storch, H., and J. Xu, 1990, Principal Oscillation Pattern analysis of the tropical 30- to 60-day oscillation. Part I: Definition on an index and its prediction. *Clim. Dyn.* 4, 175-190.

von Storch, H., U. Weese and J. Xu, 1990, Simultaneous analysis of space-time variability: Principal Oscillation Patterns and Principal Interaction Patterns with applications to the Southern Oscillation. *Z. Meteor.* 40, 99-103.

von Storch, H., and D. Baumhefner, 1991, Principal Oscillation Pattern analysis of the tropical 30- to 60-days oscillation. Part II: The prediction of equatorial velocity potential and its skill. *Clim. Dyn.* 5, 1-12.

von Storch, H., and A. Smallegange, 1991, The phase of the 30- to 60-day oscillation and the genesis of tropical cyclones in the Western Pacific. Max Planck Institut für Meteorologie Report 64 (Max-Planck-Institut. für Meteorologie, Bundesstrasse 55, 2000 Hamburg 13, Germany).

Wallace, J.M. and R E. Dickinson, 1972, Empirical orthogonal representation of time series in the frequency domain. Part I: Theoretical considerations. *J. Appl. Meteor.* 11, 887- 892.

Weisse, R., U. Mikolajewicz and E. Maier-Reimer, Decadal variability of the Northern North Atlantic in an Ocean General Circulation Model. *J. Geophys. Res.* (in press).

Wright, P., 1985, The Southern Oscillation—An ocean-atmosphere feedback system? *Bull. Am. Met. Soc.* 66, 398-412.

Xu, J., 1990, Analysis and prediction of the El Niño Southern Oscillation phenomenon using Principal Oscillation Pattern Analysis. Max Planck Institut für Meteorologie Examensarbeiten 4 (Max-Planck-Institut für Meteorologie; Bundesstrasse 55; 2000 Hamburg 13, Germany).

Xu, J., 1992, On the relationship between the stratospheric QBO and the tropospheric SO. *J. Atmos. Sci.* 49, 725-734.

Xu, J., 1993, The observed global low frequency variability in the atmosphere-ocean system from 1967 to 1986. *J. Climate* 6, 816-838.

Xu, J. and H. von Storch, 1990, "Principal Oscillation Patterns"-prediction of the state of ENSO. *J. Climate* 3, 1316-1329.